A reciprocal theorem for biphasic poro-viscoelastic materials

Moslem Moradi^{1,2}, Wenzheng Shi¹, and Ehssan Nazockdast¹†

¹Department of Applied Physical Sciences, University of North Carolina at Chapel Hill, Chapel Hill, NC 27599-3250, USA

²Department of Chemical Engineering, University of Pittsburgh, Pittsburgh, PA 15261, USA

(Received xx; revised xx; accepted xx)

In studying the transport of inclusions in multi-phase systems we are often interested in integrated quantities such as the net force and the net velocity of the inclusions. In the reciprocal theorem, the known solution to the first and typically easier boundary value problem is used to compute the integrated quantities, such as the net force, in the second problem without the need to solve that problem. Here, we derive a reciprocal theorem for poro-viscoelastic (or biphasic) materials which are composed of a linear compressible solid phase, permeated by a viscous fluid. As an example, we analytically calculate the time-dependent net force on a rigid sphere in response to point-forces applied to the elastic network and the Newtonian fluid phases of the biphasic material. We show that when the point-force is applied to the fluid phase, the net force on the sphere evolves over timescales that are independent of the distance between the point-force and the sphere; in comparison, when the point-force is applied to the elastic phase the timescale for force development increases quadratically with the distance, in line with the scaling of poroelastic relaxation time. Finally, we formulate and discuss how the reciprocal theorem can be applied to other areas, including (i) calculating the network slip on the sphere's surface, (ii) computing the leading order effects of nonlinearities in the fluid and network forces and stresses, and (iii) calculating self-propulsion in biphasic systems.

1. Introduction

Multiphase systems composed of deformable solid structures permeated by fluids are found in many natural and industrial settings, including flow and mass transport in soils and rocks (Cheng 2016), and polymer gels (Doi 2009). The main focus on this paper is on biological materials that are composed of flexible filamentous networks permeated by a fluid-like phase (Burla et al. 2019), including tissues (Cowin & Doty 2007), the cell cytoskeleton (Howard 2001) and the nucleus (Kalukula et al. 2022; Hobson et al. 2021). In many processes, the mechanical deformations coincide with volumetric contraction and expansion of the skeleton. These volumetric deformations drive interstitial fluid flows, similar to those we observe when we squeeze a wet sponge. When the network (the solid skeleton hereafter referred to as the network) is incompressible and obey no-slip boundary conditions (BCs), the fluid and the network phase co-move and the displacement field relaxation dynamics is uniform across the space in both phases. In contrast, the relaxation of the fluid pressure and network isotropic stress induced by volumetric deformations follows a diffusion process and, thus, increases quadratically with the distance from the applied force/stress (Doi 2009). Studies in recent years have shown that this distinct poroelastic relaxation time plays a key role in several cellular

processes. For example, poroelastic relaxation time is argued to set a constraint on the rate of swelling and mechanical response of plant cells (Dumais & Forterre 2012; Forterre 2022), and contraction of muscle fibers (Shankar & Mahadevan 2022). The relaxation dynamics of interstitial fluid flows is also key to determining the dynamics of cells under osmotic perturbations (Esteki et al. 2021; Jiang & Sun 2013; Moeendarbary et al. 2013) and blebbing of the plasma membrane (Charras et al. 2005, 2008; Mitchison et al. 2008; Strychalski et al. 2015).

Biot theory of poroelasticity (Biot 1941, 1955) is a well-established framework for studying biphasic materials. In this model, the fluid and elastic phases are coupled through a friction term that is linearly proportional to the relative velocity of the phases, and the fluid shear stresses are assumed to be negligible. Therefore, the fluid momentum equation is described by Darcy's equation. This is a reasonable assumption, when studying the mechanical response in a homogeneous systems over lengthscales much larger than the mesh size of the network. However, for the reasons outlined in the next two paragraphs, shear stresses must be included in many cellular materials, and Brinkman equation is more suitable for modeling fluid momentum equation.

The semi-flexible filament networks in biological materials often constitute a very small volume fraction of the system. Scaling analysis shows that Brinkman equation is a more accurate description of the fluid flows than Darcy's equation, when the volume fraction of the network is very small (Auriault 2009; Lévy 1983). Furthermore, in many instances, e.g. in the cell nucleus (Cremer et al. 2020), the underlying poroelastic materials can be highly heterogeneous, made of more fluid-like domains with large permeability, to domains that are packed with the network phase. The size of these domains can be comparable in size to the network mesh size. Brinkman equation has the advantage of asymptoting to correct limits of Stokes flow in network-free phases and Darcy's equation in small permeability. It also provides a natural framework for imposing physically consistent BCs at interfaces, where fluid shear forces cannot be ignored (Carrillo & Bourg 2019; Carrillo et al. 2020) and computing intracellular and intranuclear fluid flows.

Another example, where Brinkman equation provides clear advantages over Darcy's equation, is in studying the time-dependent response of the biological materials in microrheological techniques. As discussed in details in Levine & Lubensky (2000, 2001) and Moradi et al. (2022), at times smaller than the poroelastic relaxation time in the scale of the particle, $\tau^* = a^2 \xi/(2G + \lambda)$, the network and fluid phases co-move and the viscoelastic response of a biphasic material is determined only by the elastic and viscous shear stresses. Here, G and λ are the first and second Lamé coefficients of the network, and ξ is the friction coefficient that relates the frictional body force to the relative motion of the fluid and the network phase. In this limit, Generalized Stokes-Einstein (GSE) relationship can be used to determine the rheology. These shear relaxation modes are absent in Biot theory. In comparison, pressure-driven fluid flows induced by the network compressibility develop at $t \geq \tau^*$ and lead to a slower distance-dependent relaxation dynamics that is captured using Biot theory, and not in GSE framework (Moradi et al. 2022). Brinkman equation allows us to study the dynamics across different timescales and lengthscales.

The biopolyemric networks are heterogeneous and are filled with other bodies, such as organelles and vesicles in the cell cytoplasm, cells moving through the extracellular matrix, and the cell nucleus within the cell itself. The transport of these bodies is to a great extent determined by their mediated mechanical interactions with the network and the fluid phases. Assuming that the solid and fluid phases can be described as linear viscoelastic materials, the conservation equations reduce to two coupled linear homogeneous elliptic PDEs and a mass conservation. Computing these interactions

requires solving the PDEs, subject to appropriate BCs on the surface of all the involved domains. Finite element (Simon 1992) and immersed boundary (Strychalski *et al.* 2015) methods have been used solve these PDEs.

A similar mathematical problem arises in Stokes flow, when studying the transport of inclusions. There, the linear homogeneous elliptic form of the momentum equation for velocity allows one to develop robust mathematical formulations and numerical recipes for solving these boundary value problems (Happel & Brenner 2012; Kim & Karrila 2013), providing massive improvement in efficiency compared to FEM and other PDE solvers that require discretization of the computational domain. A few important examples are Stokesian Dynamics used for modeling suspensions of rigid particles (Brady & Bossis 1988; Fiore & Swan 2019) and boundary integral methods (Pozrikidis 1992, 2002) that allow modeling deformable bodies with complex geometry.

Our main objective is to develop a similar set of tools for linear poro-viscoelastic (PVE) or biphasic materials, to study transport problems in intracellular and extracellular assemblies of filaments and biopolyemrs. These tools rest on three mathematical results in Stokes flow: general solutions to the equations of motion, known as Lamb's general solution; fundamental solutions *i.e.* free space Green's function, of point-forces and higher order singularities; and the Lorentz's reciprocal theorem. In an earlier study (Moradi *et al.* 2022), we presented the general solutions for PVE materials. The fundamental solutions have been also been calculated (Levine & Lubensky 2000, 2001). Here, we develop the other piece of this mathematical framework by formulating the reciprocal theorem for this class of materials.

The reciprocal theorem appears in different areas of physics and engineering, surveyed in Masoud & Stone (2019). The main idea in reciprocal theorem is that the solutions to an auxiliary problem under a given set of boundary conditions (BCs) can be used to obtain the solutions under another more complex set of BCs without having to solve the boundary value problem. The auxiliary problem must be sufficiently simple to obtain closed-form solutions. Because of the linearity of the equations, the reciprocal theorem implies that the relation between kinetics and kinematics is linear and the response functions must be symmetric (Lauga & Powers 2009). Apart from its mathematical elegance, the reciprocal theorem is useful in determining the motion of microswimmers in bulk Newtonian and viscoelastic fluids (Becker et al. 2003; Li et al. 2021; Elfring 2015; Lauga & Powers 2009), and propulsion of particles at liquid-gas interfaces (Stone & Samuel 1996; Masoud & Stone 2014; Elfring et al. 2016), among other things (Masoud & Stone 2019).

The integral representation for the unknown variables are also the restatement of the governing equations from a three-dimensional PDE to a two-dimensional integral equation for unknown densities over the boundary of the fluid domain, which forms the basis of boundary integral numerical methods (Pozrikidis 2002). A reciprocal theorem has been developed for Biot consolidation theory and used to formulate boundary integral equations for Biot theory (Predeleanu 1984; Cheng & Predeleanu 1987; Detournay & Cheng 1993). The present work generalizes this reciprocal theorem to biphasic systems with non-negligible fluid shear stresses.

The paper is organized as follows. In section §2, we present the governing equations for linear PVE materials followed by the derivation for the reciprocal theorem. In section §3 we use the reciprocal theorem to derive analytical expressions for the net force on a rigid stationary sphere in response to point-forces in the Newtonian fluid phase and the linear compressible elastic network phase of a linear PVE material. In section §4, we discuss some other applications of the reciprocal theorem. Specifically, we present formulations that allow (1) calculating of the leading order effects of network slip on the response

of a sphere under a prescribed force/velocity, (2) computing the leading order effects of nonlinear terms in forces and stresses in both phases, and (3) calculating self-propulsion speed of active microswimmers in biphasic systems. The summary of our results and brief discussions on other applications of the reciprocal theorem are presented in section §5.

2. Governing equations and the reciprocal theorem

The conservation equations for a two-phase system composed of a dilute network phase permeated by a fluid phase are:

Mass conservation:
$$\nabla \cdot (\phi \mathbf{v}_n + (1 - \phi)\mathbf{v}_f) = 0,$$
 (2.1a)

Momentum Eq. for the fluid:
$$\nabla \cdot (\boldsymbol{\sigma}_f - (1 - \phi)p\mathbf{I}) + \xi (\boldsymbol{v}_f - \boldsymbol{v}_n) + \mathbf{f}_f = \mathbf{0}$$
, (2.1b)

Momentum Eq. for the network:
$$\nabla \cdot (\boldsymbol{\sigma}_n - \phi p \mathbf{I}) - \xi (\boldsymbol{v}_f - \boldsymbol{v}_n) + \mathbf{f}_n = \mathbf{0},$$
 (2.1c)

where subscripts n and f denote network and fluid phases, $\phi \ll 1$ is the volume fraction of the network phase, σ_n is the network stress, p is the pressure that ensures fluid incompressibility constraint; ξ is the friction constant per unit volume of the material, \mathbf{f}_f , and \mathbf{f}_n are the external body forces on the network and fluid phases, respectively, and \mathbf{I} is the identity matrix. We take the volume fraction of the network phase, ϕ , to remain constant in space and time. Thus, the compressibility of the network leads to nonzero divergence of the fluid velocity field: $\nabla \cdot \mathbf{v}_f = (\phi/(1-\phi))\nabla \cdot \mathbf{v}_n \neq 0$. However, this apparent fluid compressibility is not associated with changes in fluid density and arises from fluid sources and sinks in response to changes in volume of the network phase. As such, the Newtonian fluid stress does not include the isotropic term that scales with η_b ($\nabla \cdot \mathbf{v}_f$), where η_b is the bulk viscosity. We use a general linear viscoelastic (VE) isotropic constitutive equation to describe the traceless part of the fluid stress:

$$\boldsymbol{\sigma}_f = \int_0^t G_f(t - t') \left(\nabla \boldsymbol{v}_f(t') + \nabla \boldsymbol{v}_f^T(t') \right) dt', \tag{2.2}$$

where $G_f(t)$ is the fluid's shear modulus. Similarly, we model the network stress, σ_n , using a general linear VE constitutive equation:

$$\boldsymbol{\sigma}_n = \int_0^t \mathbf{C}(t - t') : \left(\nabla \boldsymbol{v}_n(t') + \nabla \boldsymbol{v}_n^T(t') \right) dt', \tag{2.3}$$

where $\mathbf{C}(t)$ is the symmetric fourth-rank stiffness tensor[†], and ":" is double dot product. Taking Laplace transform of Eqs. (2.2) and (2.3) gives $\tilde{\boldsymbol{\sigma}}_f = \tilde{\eta}(s) \left(\nabla \tilde{\boldsymbol{v}}_f + \nabla \tilde{\boldsymbol{v}}_f^T\right)$ and $\tilde{\boldsymbol{\sigma}}_n = \tilde{\mathbf{C}}(s) : \left(\nabla \tilde{\boldsymbol{v}}_n + \nabla \tilde{\boldsymbol{v}}_n^T\right)$, where superscripts \sim denote variables in Laplace space, and $\tilde{\eta}(s) = \mathcal{L}(G_f(t))$, where \mathcal{L} is the Laplace transform operator. Taking Laplace transform of Eqs. (2.1) and using convolution theorem we get:

$$\nabla \cdot (\tilde{\boldsymbol{v}}_n \phi + \tilde{\boldsymbol{v}}_f (1 - \phi)) = 0, \tag{2.4a}$$

$$\nabla \cdot \tilde{\Sigma}_f + \xi(\tilde{v}_n - \tilde{v}_f) = -\tilde{\mathbf{f}}_f, \qquad (2.4b)$$

$$\nabla \cdot \tilde{\boldsymbol{\Sigma}}_n - \xi(\tilde{\boldsymbol{v}}_n - \tilde{\boldsymbol{v}}_f) = -\tilde{\mathbf{f}}_n, \tag{2.4c}$$

† The general form of the tensor C is defined by a linear relation between stress and strain tensor as $\sigma_{ij} = C_{ijk\ell}e_{k\ell}$ and has symmetry properties due to symmetries of stress and strain tensors, so that $C_{ijk\ell} = C_{jik\ell}$ and $C_{ijk\ell} = C_{ji\ell k}$. Also, since the strain energy density is $W = \frac{1}{2}\sigma_{ij}e_{ij} = \frac{1}{2}C_{ijk\ell}e_{ij}e_{k\ell}$, we see that tensor C has reciprocal symmetry, i.e. $C_{ijk\ell} = C_{k\ell ij}$. For an isotropic tensor, only two independent constants remain: $C_{ijk\ell} = \lambda \delta_{ij}\delta_{k\ell} + G(\delta_{ik}\delta_{j\ell} + \delta_{i\ell}\delta_{jk})$, where λ and G are Lamé constants.

where $\tilde{\Sigma}_f = \tilde{\sigma}_f - (1 - \phi)\tilde{p}\mathbf{I}$ and $\tilde{\Sigma}_n = \tilde{\sigma}_n - \phi \tilde{p}\mathbf{I}$ are the total stresses in the fluid and network phases in Laplace space. Hereafter, we drop the superscript \sim in the equations, noting that all the variables are in Laplace space, unless explicitly mentioned otherwise. We take the variables with superscript $\hat{}$ and no superscript to denote two independent solutions to the above system of equations, i.e., $(\hat{v}_{\{f,n\}}, \hat{\Sigma}_{\{f,n\}})$, and $(v_{\{f,n\}}, \Sigma_{\{f,n\}})$, with the corresponding body forces $\hat{\mathbf{f}}_{\{f,n\}}$ and $\mathbf{f}_{\{f,n\}}$, respectively; then, we take the dot product of Eqs (2.4b) and (2.4c), with v_f and v_n , respectively, to get:

$$\mathbf{v}_f \cdot \left[\nabla \cdot \hat{\mathbf{\Sigma}}_f + \xi \left(\hat{\mathbf{v}}_n - \hat{\mathbf{v}}_f \right) \right] = -\mathbf{v}_f \cdot \hat{\mathbf{f}}_f,$$
 (2.5a)

$$\mathbf{v}_n \cdot \left[\nabla \cdot \hat{\mathbf{\Sigma}}_n - \xi \left(\hat{\mathbf{v}}_n - \hat{\mathbf{v}}_f \right) \right] = -\mathbf{v}_n \cdot \hat{\mathbf{f}}_n.$$
 (2.5b)

We repeat the same process, using the solution $(\boldsymbol{v}_{\{f,n\}}, \boldsymbol{\Sigma}_{\{f,n\}})$ with the corresponding body force, $\mathbf{f}_{\{f,n\}}$, of Eqs. (2.4b), and (2.4c) and multiplying them by $\hat{\boldsymbol{v}}_f$ and $\hat{\boldsymbol{v}}_n$, respectively, to get:

$$\hat{\boldsymbol{v}}_f \cdot \left[\nabla \cdot \boldsymbol{\Sigma}_f + \xi \left(\boldsymbol{v}_n - \boldsymbol{v}_f \right) \right] = -\hat{\boldsymbol{v}}_f \cdot \mathbf{f}_f, \tag{2.6a}$$

$$\hat{\boldsymbol{v}}_n \cdot \left[\nabla \cdot \boldsymbol{\Sigma}_n - \xi \left(\boldsymbol{v}_n - \boldsymbol{v}_f \right) \right] = -\hat{\boldsymbol{v}}_n \cdot \mathbf{f}_n. \tag{2.6b}$$

Subtracting Eq. (2.5a) with (2.6a), and also Eq. (2.5b) with (2.6b) gives:

$$\nabla \cdot \left(\hat{\boldsymbol{\Sigma}}_{f} \cdot \boldsymbol{v}_{f} - \boldsymbol{\Sigma}_{f} \cdot \hat{\boldsymbol{v}}_{f}\right) + \xi \left[\boldsymbol{v}_{f} \cdot (\hat{\boldsymbol{v}}_{n} - \hat{\boldsymbol{v}}_{f}) - \hat{\boldsymbol{v}}_{f} \cdot (\boldsymbol{v}_{n} - \boldsymbol{v}_{f})\right]$$

$$+ (1 - \phi) \left(\hat{p}\nabla \cdot \boldsymbol{v}_{f} - p\nabla \cdot \hat{\boldsymbol{v}}_{f}\right) = \hat{\boldsymbol{v}}_{f} \cdot \mathbf{f}_{f} - \boldsymbol{v}_{f} \cdot \hat{\mathbf{f}}_{f},$$

$$\nabla \cdot \left(\hat{\boldsymbol{\Sigma}}_{n} \cdot \boldsymbol{v}_{n} - \boldsymbol{\Sigma}_{n} \cdot \hat{\boldsymbol{v}}_{n}\right) - \xi \left[\boldsymbol{v}_{n} \cdot (\hat{\boldsymbol{v}}_{n} - \hat{\boldsymbol{v}}_{f}) - \hat{\boldsymbol{v}}_{n} \cdot (\boldsymbol{v}_{n} - \boldsymbol{v}_{f})\right]$$

$$+ \phi \left(\hat{p}\nabla \cdot \boldsymbol{v}_{n} - p\nabla \cdot \hat{\boldsymbol{v}}_{n}\right) = \hat{\boldsymbol{v}}_{n} \cdot \mathbf{f}_{n} - \boldsymbol{v}_{n} \cdot \hat{\mathbf{f}}_{n}.$$

$$(2.7a)$$

Here, we have used the identities $\mathbf{v} \cdot (\nabla \cdot \mathbf{\Sigma}) = \nabla \cdot (\mathbf{\Sigma} \cdot \mathbf{v}) - \mathbf{\Sigma} : \nabla \mathbf{v}$ and $\hat{\boldsymbol{\sigma}} : \nabla \mathbf{v} = \boldsymbol{\sigma} : \nabla \hat{\mathbf{v}}$, which results from linear elastic constitutive law. Adding Eqs. (2.7a) and (2.7b), directly cancels the second terms on the left hand side, and using continuity equation $((1 - \phi)\nabla \cdot \mathbf{v}_f + \phi\nabla \cdot \mathbf{v}_n = 0)$ cancels the terms involving $p_{\{f,n\}} (\nabla \cdot \mathbf{v}_{\{f,n\}})$. The final result is the differential form of the reciprocal relations:

$$\nabla \cdot \left(\hat{\boldsymbol{\Sigma}}_{f} \cdot \boldsymbol{v}_{f} + \hat{\boldsymbol{\Sigma}}_{n} \cdot \boldsymbol{v}_{n} \right) + \hat{\boldsymbol{v}}_{f} \cdot \mathbf{f}_{f} + \hat{\boldsymbol{v}}_{n} \cdot \mathbf{f}_{n} = \nabla \cdot \left(\boldsymbol{\Sigma}_{f} \cdot \hat{\boldsymbol{v}}_{f} + \boldsymbol{\Sigma}_{n} \cdot \hat{\boldsymbol{v}}_{n} \right) + \boldsymbol{v}_{f} \cdot \hat{\mathbf{f}}_{f} + \boldsymbol{v}_{n} \cdot \hat{\mathbf{f}}_{n}.$$

$$(2.8)$$

Next, we select a control volume V, that is bounded by a closed (simply- or multiply-connected) surface $S = S_p + S_{\infty}$; see figure 1. After integrating Eq. (2.8) over V and using the divergence theorem we get

$$\int_{S_p} \left(\hat{\boldsymbol{\Sigma}}_f \cdot \boldsymbol{v}_f + \hat{\boldsymbol{\Sigma}}_n \cdot \boldsymbol{v}_n \right) \cdot \mathbf{n} \, dS + \int_V \left(\hat{\boldsymbol{v}}_f \cdot \mathbf{f}_f + \hat{\boldsymbol{v}}_n \cdot \mathbf{f}_n \right) dV
= \int_{S_p} \left(\boldsymbol{\Sigma}_f \cdot \hat{\boldsymbol{v}}_f + \boldsymbol{\Sigma}_n \cdot \hat{\boldsymbol{v}}_n \right) \cdot \mathbf{n} \, dS + \int_V \left(\boldsymbol{v}_f \cdot \hat{\mathbf{f}}_f + \boldsymbol{v}_n \cdot \hat{\mathbf{f}}_n \right) dV. \tag{2.9}$$

Equation (2.9) is the reciprocal theorem for poro-viscoelastic (PVE) materials we set out to derive, and the main result of this work. The theorem reduces to the reciprocal theorem for Biot consolidation theory (Predeleanu 1984; Cheng & Predeleanu 1987), if the fluid stress is approximated by only the isotropic pressure component and the deviatoric stress components, which corresponds to shear stresses, are dropped. Note that we have made no assumption about material isotropy up to this point, and the derived reciprocal

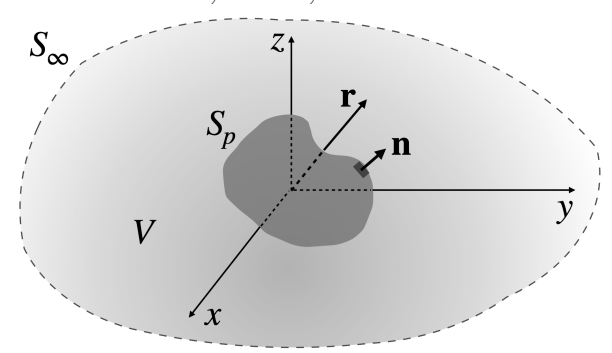


FIGURE 1. A schematic of an arbitrarily shaped inclusion, with surface S_p and unit outward normal vector \mathbf{n} , in an unbounded domain. The dashed line indicates an enclosing boundary in the "far field".

relationship also applies to linear anisotropic materials. For a linear isotropic material, the network stress in Laplace space simplifies to $\sigma_n(s) = G(s) \left(\nabla \boldsymbol{v}_n + \nabla \boldsymbol{v}_n^T \right) + \lambda(s) \left(\nabla \cdot \boldsymbol{v}_n \right)$, where, G(s) and $\lambda(s)$ are the Laplace transforms of the time-dependent first and second Lamé coefficients. For a linear elastic network (no viscous component) these coefficients are related through the Poisson ratio, ν : $\lambda = \frac{2G\nu}{1-2\nu}$.

3. The force on a rigid sphere due to point-forces in fluid and network phases

A consequence of the linearity of the governing equations is that any ambient displacement field can be expressed with a distribution of point-forces in the fluid and network domains. This also includes the active stresses in cellular materials (used to maintain and rearrange their structures) that are typically described with distribution of forces, and force-dipoles on the fluid and network phases in the continuum scale (Marchetti et al. 2013; Saintillan & Shelley 2015). Similarly, the presence of other immersed objects in a biphasic material can be modeled by distributions of point-forces and higher order singularities. In many instances the transport in cellular filamentous networks involve spherical (or sphere-like) objects, e.g. cell migration through the extracellular matrix (Camley & Rappel 2017), organelle transport throughout the cytoskeleton (Mogre et al. 2020), and the dynamics of microinjected or endogenous probes in particle tracking microscopy (Weihs et al. 2006). In these applications one must consider the movements of the spheres in response to active or passive forces/stresses in the medium. Motivated by this, and to show the utility of the reciprocal theorem, we consider a rigid spherical inclusion moving with a prescribed velocity U in a PVE medium, subject to point-forces $\mathbf{f}_{\{f,n\}}$ applied to fluid and network phases at some separation distance, \mathbf{R} , from the center of the sphere. Our goal to derive a closed-form expression for the net force, F, on the sphere in response to those point-forces; see Fig. 2(a) for a schematic of this problem.

We assume the network is a linear elastic material with shear modulus G and Poisson ratio ν , and the permeating fluid is Newtonian with shear viscosity η , so that $\tau(s) = s\eta/G = s\tau_0$, where $\tau_0 = \eta/G$ is the shear relaxation time of the network in the fluid phase. However, the expressions that we are about to present are extendable to any other linear viscoelastic fluids and networks by modifying the expression for $\tau(s)$ in terms of constitutive parameters of the two phases. The flow fields and the net forces on the particle are first computed in Laplace space. We use Fourier–Euler summation ((Abate & Whitt 1992)) to numerically invert the results from s-space to time-space.

The relative error of the numerical inversion is smaller than 10^{-9} in all the presented results.

To use the reciprocal theorem we need a simple auxiliary problem, which gives us $\hat{\boldsymbol{v}}_{\{f,n\}}$ and $\hat{\boldsymbol{\Sigma}}_{\{f,n\}}$. We choose a sphere translating with velocity $\hat{\mathbf{U}}$ as our auxiliary problem. We derived these solutions in Moradi *et al.* (2022). Since the general solution is axisymmetric (see Appendix A), it can be expressed in the general form of

$$\hat{\boldsymbol{v}}_{f} = \hat{\mathbf{U}} \cdot \left[A_{f} \frac{\mathbf{r}\mathbf{r}}{r^{2}} + B_{f} \left(\mathbf{I} - \frac{\mathbf{r}\mathbf{r}}{r^{2}} \right) \right], \qquad \hat{\boldsymbol{v}}_{n} = \hat{\mathbf{U}} \cdot \left[A_{n} \frac{\mathbf{r}\mathbf{r}}{r^{2}} + B_{n} \left(\mathbf{I} - \frac{\mathbf{r}\mathbf{r}}{r^{2}} \right) \right], \quad (3.1a)$$

$$\hat{p} = A_{p} \hat{\mathbf{U}} \cdot \frac{\mathbf{r}}{r}. \quad (3.1b)$$

Applying the BCs, $\hat{\boldsymbol{v}}_f\big|_{r=a} = \hat{\mathbf{U}}$, and $\hat{\boldsymbol{v}}_n\big|_{r=a} = \hat{\mathbf{U}}$, specifies, $A_{\{f,n\}}$ and $B_{\{f,n\}}$ as follows:

$$A_f = \frac{1}{\Delta} \left[S_1(\frac{a}{r}) + S_2(\frac{a}{r})^3 - 3\frac{a\alpha^2}{\beta^4 r^3} (1 + \beta r) e^{-\beta(r-a)} \right], \tag{3.2a}$$

$$B_f = \frac{1}{\Delta} \left[S_1(\frac{a}{r}) - S_2(\frac{a}{r})^3 + 3\frac{a\alpha^2}{\beta^4 r^3} (1 + \beta r + \beta^2 r^2) e^{-\beta(r-a)} \right], \tag{3.2b}$$

$$A_{n} = \frac{1}{\Delta} \left[S_{1} \left(\frac{a}{r} \right) - S_{3} \left(\frac{a}{r} \right)^{3} + 3\tau \frac{a\alpha^{2}}{\beta^{4} r^{3}} (1 + \beta r) e^{-\beta(r-a)} + 3 \frac{a(1+\tau)}{\beta^{2} r^{3}} e^{-\alpha(r-a)} \right]$$

$$\times (2 + 2\alpha r + \alpha^{2} r^{2}),$$
(3.2c)

$$B_{n} = \frac{1}{\Delta} \left[S_{1} \left(\frac{a}{r} \right) + S_{3} \left(\frac{a}{r} \right)^{3} - 3\tau \frac{a\alpha^{2}}{\beta^{4} r^{3}} (1 + \beta r + \beta^{2} r^{2}) e^{-\beta(r-a)} - 6 \frac{a(1+\tau)}{\beta^{2} r^{3}} e^{-\alpha(r-a)} \right] \times (1 + \alpha r),$$

$$(3.2d)$$

$$A_p = \frac{G}{a\Delta} \left[\frac{1+\tau}{3} S_1 \left(\frac{a}{r} \right)^2 - 3\tau \left(\frac{a}{r} \right)^2 (1+\alpha r) e^{-\alpha(r-a)} \right], \tag{3.2e}$$

where

$$S_{1} = 3\tau \left(1 + a\alpha + \frac{1}{2}\frac{\alpha^{2}}{\beta^{2}}(1 + a\beta + a^{2}\beta^{2})\right), \quad S_{2} = \frac{\alpha^{2}}{a^{2}\beta^{4}}(3 + 3a\beta + a^{2}\beta^{2}) - \frac{1}{3}S_{1}, (3.3a)$$

$$S_{3} = \frac{2}{a^{2}\beta^{2}}(3 + 3a\alpha + a^{2}\alpha^{2}) + \frac{6 + a^{2}\beta^{2}}{3a^{2}\beta^{2}}S_{1}, \quad \Delta = \frac{\alpha^{2}}{\beta^{2}} + \frac{2}{3}S_{1}. \tag{3.3b}$$

Here, $\beta^2 = \beta_o^2 (1+\tau)$, with $\beta_o = \sqrt{\frac{\xi}{\eta}}$ being the inverse of permeability of the fluid and $\alpha^2 = s\tau_o\alpha_o^2$, where $\alpha_o^2 = \beta_o^2 \frac{1-2\nu}{2(1-\nu)}$ with ν being the Poisson ratio. For an incompressible network, $\nu = 0.5$ and $\alpha_o = 0$. Substituting these values in the above equations cancels all the terms involving β_o and reduces the expressions for $A_{\{f,n\}}$ and $B_{\{f,n\}}$ in Eqs. (3.2), to their well-known form in Stokes flow:

$$\begin{split} A_{\{f,n\}}(\nu = 0.5) &= A_{\rm Stokes} = \frac{3}{2} \left(\frac{a}{R}\right) - \frac{1}{2} \left(\frac{a}{R}\right)^3, \\ B_{\{f,n\}}(\nu = 0.5) &= B_{\rm Stokes} = \frac{3}{4} \left(\frac{a}{R}\right) + \frac{1}{4} \left(\frac{a}{R}\right)^3. \end{split}$$

We are interested in the dynamical features that arise due to network compressibility. Using the expressions in Eq. (3.1b), we can compute the traction applied by the fluid and the network phase on the surface of the sphere and integrate those on the sphere's

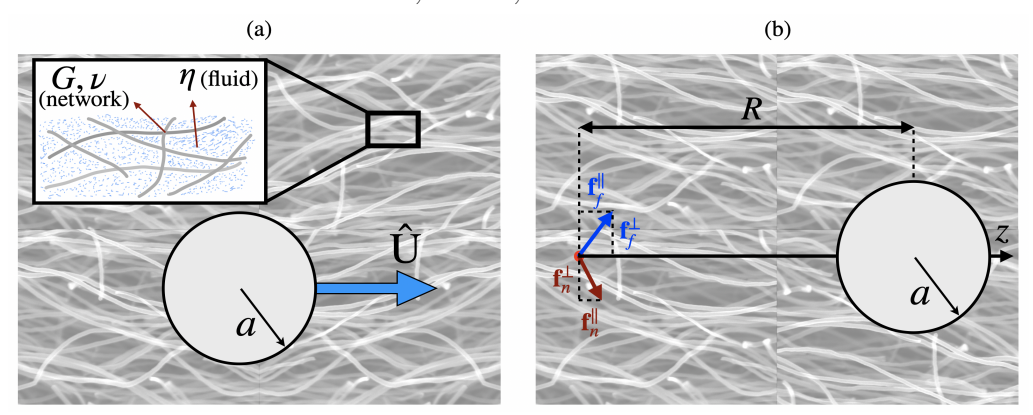


FIGURE 2. (a) The auxiliary problem in the implementation of the reciprocal theorem: A rigid sphere moving with a prescribed velocity $\hat{\mathbf{U}}$ in a linear PVE medium with fluid shear viscosity η and network shear modulus G and Poison ratio ν . (b) The problem to be solved using reciprocal theorem: a rigid sphere moving with a prescribed velocity and subjected to external point-forces in the fluid and the network phases, \mathbf{f}_f , and \mathbf{f}_n .

surface to get the net force on the particle:

$$\hat{\mathbf{F}} = \int \left(\hat{\mathbf{\Sigma}}_f + \hat{\mathbf{\Sigma}}_n \right) \cdot \mathbf{n} \, dS \equiv -\mathcal{R} \, \hat{\mathbf{U}}, \tag{3.5}$$

$$\mathcal{R} = 6\pi \eta a \left[\frac{(1+\tau) \left(\alpha^2 \left(a^2 \beta^2 + a\beta + 1 \right) + 2\beta^2 (1+a\alpha) \right)}{\tau \left(\alpha^2 \left(a^2 \beta^2 + a\beta + 1 \right) + 2\beta^2 (1+a\alpha) \right) + \alpha^2} \right].$$

The term between brackets is the correction to Stokes drag induced by network compressibility.

The second problem is the problem we seek to solve, which is shown in Fig. 2(b). We assume no-slip BCs for both the fluid and network on the surface of the sphere: $v_{\{f,n\}}(r=a) = \mathbf{U}$. No-slip BCs is generally valid for the fluid phase. The BCs for the network phase is more complex (Fu et al. 2010). When the particle size is much larger than the network's mesh size, $a\beta_{\circ} \gg 1$, the no-slip BC is a good approximation. This is the BC used in this section. In section §4.1 we discuss how the reciprocal theorem can be used to compute the leading order effect of network slip on the dynamics of the sphere.

The point-forces are expressed as $\mathbf{f}_f = \mathbf{f}_f^{\circ} \delta(\mathbf{r} - \mathbf{R})$ and $\mathbf{f}_n = \mathbf{f}_n^{\circ} \delta(\mathbf{r} - \mathbf{R})$, where $\delta(\mathbf{r} - \mathbf{R})$ is the Dirac delta function. After substituting these expressions in Eq. (2.9) and a few simple lines of algebra we get

$$-\mathcal{R}\mathbf{U} + \mathcal{M}_f \cdot \mathbf{f}_f^{\circ} + \mathcal{M}_n \cdot \mathbf{f}_n^{\circ} = \mathbf{F}, \tag{3.6}$$

where

$$\mathcal{M}_f = A_f(R) \frac{\mathbf{R}\mathbf{R}}{R^2} + B_f(R) \left(\mathbf{I} - \frac{\mathbf{R}\mathbf{R}}{R^2}\right), \qquad \mathcal{M}_n = A_n(R) \frac{\mathbf{R}\mathbf{R}}{R^2} + B_n(R) \left(\mathbf{I} - \frac{\mathbf{R}\mathbf{R}}{R^2}\right), (3.7)$$

Equations (3.6) and (3.7) are the expressions we set out to derive. \mathcal{M}_f and \mathcal{M}_n are the response functions that relate the forces on fluid and network phases to the net force and velocity of the spherical particle. For a force-free particle (mobility problem), we can set $\mathbf{F} = 0$, which yields

Force-free particle,
$$\mathbf{F} = \mathbf{0}$$
: $\mathbf{U} = \mathcal{R}^{-1} \left(\mathcal{M}_f \cdot \mathbf{f}_f^{\circ} + \mathcal{M}_n \cdot \mathbf{f}_n^{\circ} \right),$ (3.8)

In this setup, \mathcal{M}_f and \mathcal{M}_n can be thought of as mobility tensors that relate the forces

on each phase to the particle's velocity. For brevity, we only present the results of fixed particle (resistance problem), $\mathbf{U} = \mathbf{0}$, in the next section. The solution can easily be extended to force-free particles (mobility problem), using Eq. (3.8).

Net force on a fixed sphere

We consider the special case of a fixed particle, U = 0, which simplifies Eq. (3.6) to

Fixed particle,
$$\mathbf{U} = \mathbf{0}$$
: $\mathbf{F} = \mathcal{M}_f \cdot \mathbf{f}_f^{\circ} + \mathcal{M}_n \cdot \mathbf{f}_n^{\circ}$. (3.9)

It is useful to decompose the point-forces and the force on the particle in parallel and perpendicular directions of the separation vector. Using $\mathbf{f}_{\{f,n\}}^{\circ} = \mathbf{f}_{\{f,n\}}^{\parallel} \hat{\mathbf{R}} + \mathbf{f}_{\{f,n\}}^{\perp} \hat{\mathbf{R}}^{\perp}$, and $\mathbf{F} = F^{\parallel} \hat{\mathbf{R}} + F^{\perp} \hat{\mathbf{R}}^{\perp}$ we get:

$$F^{\parallel} = A_f(R)f_f^{\parallel} + A_n(R)f_n^{\parallel}, \qquad F^{\perp} = B_f(R)f_f^{\perp} + B_n(R)f_n^{\perp}.$$
 (3.10)

We begin by analyzing the limiting behaviors of $A_{\{f,n\}}$ and $B_{\{f,n\}}$ at early $(t \to 0)$ and long $(t \to \infty)$ times. These limits can be computed analytically using the following relationships: $f(t \to 0^+) = \lim_{s \to \infty} sf(s)$ and $f(t \to \infty) = \lim_{s \to 0} sf(s)$ and the results are:

$$A_{\{f,n\}}(t \to 0) = \frac{3}{2} \left(\frac{a}{R}\right) - \frac{1}{2} \left(\frac{a}{R}\right)^{3}, \qquad B_{\{f,n\}}(t \to 0) = \frac{3}{4} \left(\frac{a}{R}\right) + \frac{1}{4} \left(\frac{a}{R}\right)^{3}, \quad (3.11a)$$

$$A_{f}(t \to \infty) = \frac{6(1-\nu)}{5-6\nu} \left(\frac{a}{R}\right) - \frac{1}{5-6\nu} \left(\frac{a}{R}\right)^{3} + \frac{3a(1-2\nu)}{\beta_{\circ}^{2} R^{3}(5-6\nu)} \left[1 + a\beta_{\circ} - (1+\beta_{\circ}R) + (3.11b)\right]$$

$$\times e^{-\beta_{\circ}(R-a)}, \qquad (3.11b)$$

$$B_{f}(t \to \infty) = \frac{3(1-\nu)}{5-6\nu} \left(\frac{a}{R}\right) + \frac{1}{2(5-6\nu)} \left(\frac{a}{R}\right)^{3} - \frac{3a(1-2\nu)}{2\beta_{\circ}^{2} R^{3}(5-6\nu)} \left[1 + a\beta_{\circ} - (1+\beta_{\circ}R) + (\beta_{\circ}R^{2}) + (\beta$$

$$B_n(t \to \infty) = \frac{3(3-4\nu)}{2(5-6\nu)} \left(\frac{a}{R}\right) + \frac{1}{2(5-6\nu)} \left(\frac{a}{R}\right)^3.$$
 (3.11e)

As shown in Eq. (3.11)(a), at short times the response functions for both fluid and network asymptote to their well-known respective forms in Stokes flow (Kim & Karrila 2013). This can be explained by noting that at early times the network co-moves with the fluid phase, $\mathbf{v}_n(\mathbf{r}, t \to 0) = \mathbf{v}_f(\mathbf{r}, t \to 0)$, and $\nabla \cdot \mathbf{v}_{\{f,n\}}(\mathbf{r}, t \to 0) = 0$. Furthermore, at long times the response functions of the network phase $(A_n \text{ and } B_n)$, approach their well-known form in linear elasticity (Phan-Thien & Kim 1994); see Eqs. (3.11)(d-e). The long time forms of the fluid response functions $(A_f \text{ and } B_f)$ include extra β_o -dependent, which, as expected, become identically zero for an incompressible network.

Variations of the net force with time and the distance from the point-forces in the parallel direction are determined by the behavior of $A_{\{f,n\}}$. Since we have the analytical form of these functions in short and long times in Eqs. (3.11), we study the time-dependent behavior of the following quantities

$$\hat{A}_{\{f,n\}} = \frac{A_{\{f,n\}}(t,R) - A_{\{f,n\}}(t \to \infty, R)}{A_{\{f,n\}}(0,R) - A_{\{f,n\}}(t \to \infty, R)}, \quad \hat{B}_{\{f,n\}} = \frac{B_{\{f,n\}}(t,R) - B_{\{f,n\}}(t \to \infty, R)}{B_{\{f,n\}}(0,R) - B_{\{f,n\}}(t \to \infty, R)}.$$
(3.12)

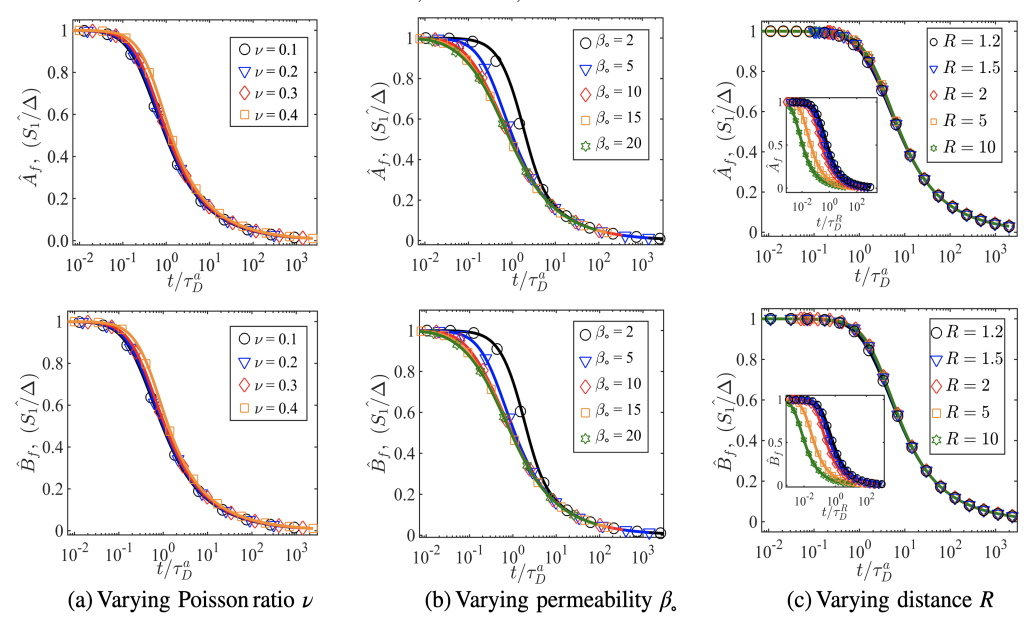


FIGURE 3. Time variations of the fluid hydrodynamic functions, \hat{A}_f (top row) and \hat{B}_f (bottom row). (a) Different values of Poisson ratio, ν , while setting $\beta_\circ = 5$ and R = 2. (b) Different values of permeability, β_\circ , while setting $\nu = 0.3$ and R = 2, and (c) different separation distances, R, while setting $\nu = 0.3$ and $\beta_\circ = 5$. The time axis is made dimensionless with $\tau_D^D = a^2\alpha_\circ^2\tau_\circ$ in all the main plots. The values of R and β_\circ are made dimensionless with the sphere radius, which is equivalent to taking a := 1. The inset figures in Fig. 3(c) show the same results as the main figure, but the time axes are made dimensionless with $\tau_D^R = R^2\alpha_\circ^2\tau_\circ$.

 \hat{A} and \hat{B} , by construction relax over time from $\hat{A} = \hat{B} = 1$ at t = 0 to $\hat{A} = \hat{B} \to 0$ as $t \to \infty$. Next, we explore how the relaxation dynamics changes with the separation distance, R, and material properties of the fluid and network, η, G, β_{\circ} and ν .

The expressions for $A_{\{f,n\}}$ and $B_{\{f,n\}}$ in Eqs. (3.2) contain two types of s and R dependencies. One obvious relaxation mechanism is shear relaxation, $\tau_{\circ} = \eta/G$, which is independent of β_{\circ} and ν and the separation distance, R. This is the relaxation time measured in the standard particle tracking microrheology. The terms involving S_1 , S_2 and S_3 can be written as a product of only s-dependent and only r-dependent function, $\tilde{\mathcal{Q}}(s)\mathcal{P}(r)$, resulting in $\mathcal{Q}(t)\mathcal{P}(r)$ form after Laplace inversion. As a result, the relaxation behavior becomes independent of R. In comparison, the terms that include $\exp(-\beta(s)r)$ and $\exp(-\alpha(s)r)$, cannot be written as a product of s- and r-dependent functions, and so the relaxation time of the force on the sphere becomes a function of the distance from the point-forces.

As shown in our earlier work (Moradi *et al.* 2022) and others (Doi 2009; Detournay & Cheng 1993) the divergence of the displacement field in a linear elastic network, $\nabla \cdot \boldsymbol{v}_n$, is described by a diffusion equation, where the diffusion coefficient is $D = \tau_o \alpha_o^{-2}$. Based on this, we can introduce two extra timescales: $\tau_D^a = (\alpha_o a)^2 \tau_o$, which is the timescale for the network compressibility to diffuse over a particle radius, a; and $\tau_D^R = (\alpha_o R)^2 \tau_o$ is the time for diffusing distance R from the point-forces.

If the S_1 , S_2 and S_3 terms dominate the response, we expect the force relaxation time to be independent of R and determined by τ_D^a ; alternatively, if $\exp(-\alpha(s)r)$ and $\exp(-\beta(s)r)$ terms determine the behavior of $A_{\{f,n\}}$ and $B_{\{f,n\}}$, we expect the force relaxation to be distance-dependent and in part determined by τ_D^R .

We begin with presenting the results for the relaxation dynamics of fluid phase functions, \hat{A}_f and \hat{B}_f vs time in Fig. 3 for different values of Poisson ratio, ν (Fig. 3(a)), permeability, β_{\circ} (Fig. 3(b)) and distance from the point-force R (Fig. 3(c)). The solid lines that go through the markers are the computed values of (S_1/Δ) , which is simply the the values of S_1/Δ made dimensionless in the exact manner as A_f and B_f in Eq. (3.2). The relaxation time is made dimensionless with τ_D^a in all figures. When R is fixed and ν and β_{\circ} are varied (Figs. 3(a-b)), τ_D^a and τ_D^B are linearly related by a constant factor, $\tau_D^R/\tau_D^a = (R/a)^2$, and using τ_D^R (instead of τ_D^a) would only shift the plots in x-axis and would not change the overall superposition of the curves. In comparison, when R is varied, the two timescales become distinct. Thus, to test if the relaxation is distance-dependent or not, we present the results of Fig. 3(c) as a function of t/τ_D^R in the insets of those figures.

As it can be seen, in all cases (S_1/Δ) (solid lines) closely match the predictions that include all the terms (symbols). This suggest that the relaxation is distance-independent and that τ_D^a (and not τ_D^R) is a more appropriate choice for relaxation time of \hat{A}_f and \hat{B}_f . This can be clearly seen by comparing the nearly perfect superposition of the plots in the main figure against the inset plots in Fig. 3(c). Furthermore, the relaxation curves for different values of ν superimpose, when time is made dimensionless with τ_D^a . The superposition is not as clean at shorter times when permeability is varied (see Fig. 3(b)), since shear relaxation time (τ_o) , becomes increasingly more important at shorter timescales, where the fluid and network phase co-move. However, at longer times $(t/\tau_D^a) \geq 10$ the plots superimpose, showing that the long time behavior of these hydrodynamic functions is determined by τ_D^a . Collectively, these results show that the relaxation dynamics of \hat{A}_f and \hat{B}_f is not distance-dependent, and is dominated by the terms involving $(S_1/\Delta)(a/r)$ and the relaxation time, τ_D^a .

Figure 4 shows the relaxation dynamics of the network functions, \hat{A}_n and \hat{B}_n . In this case, the solid lines are just showing the detailed predictions and are not showing (S_1/Δ) , since (S_1/Δ) values did not match the detailed predictions. The time axis is made dimensionless by τ_D^R in all the main plots. Again, when the separation distance is varied, we re-plot the results of Figs. 4(c) in the inset figure, but with the the dimensionless time being defined as t/τ_D^a . As it can be seen in Fig. 4(c), using t/τ_D^R gives a better collapse of the relaxation plots at long times and at different R in the main plot, compared to the inset figures, with t/τ_D^a as x-axis. However, the collapse is not as clean as the results for \hat{A}_f and \hat{B}_f . For both cases of varying permeability and distance (Figs. 4(b) and 4(c)) the plots fail to collapse at shorter times, especially for \hat{B}_n , where the shape of the plots qualitatively changes with varying β_0 and R.

All together these results suggest that the relaxation behavior of the network functions \hat{A}_n and \hat{B}_n at long times is distance-dependent and best described by τ_D^R . However, at shorter times the fluid shear stress plays a more central role and the relaxation dynamics is a function of all three timescales (τ_o , τ_D^a and τ_D^R). Including the shear stresses in the conservation equations allows us to study the complex variations in the relaxation behavior from short to long timescales.

4. Other applications

In this section, we give a brief overview of some of the other applications of the reciprocal theorem for PVE materials. Our focus here is to derive the final expressions (in form of surface and volume integrals) for each application, without evaluating these expressions and discussing the results for different choices of parameters.

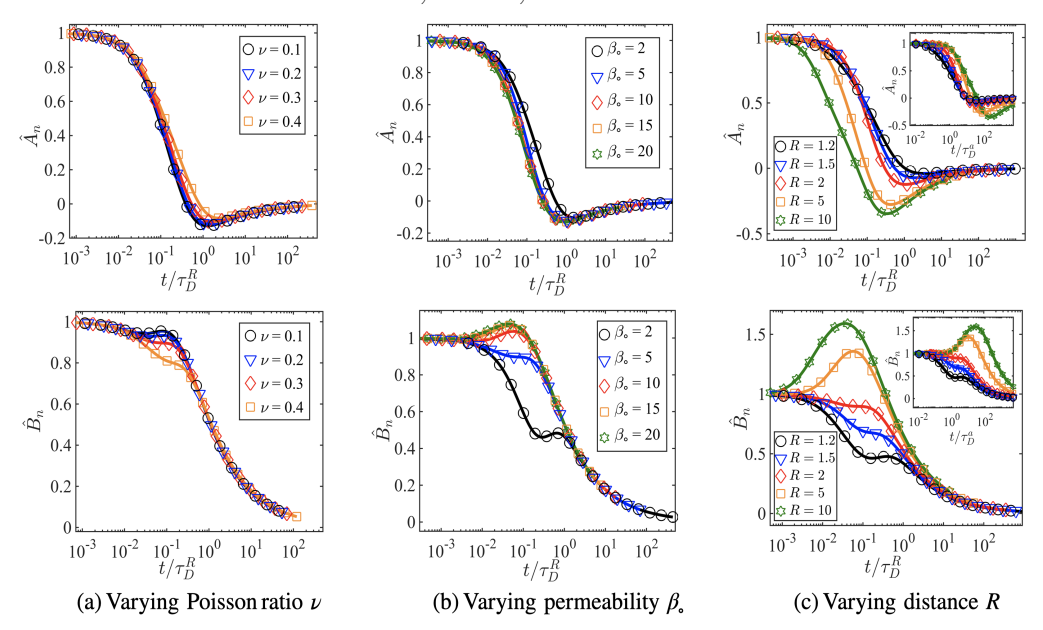


FIGURE 4. Time variations of the network hydrodynamic functions, \hat{A}_n (top row) and \hat{B}_n (bottom row). (a) Different values of Poisson ratio, ν , while setting $\beta_{\circ} = 5$ and R = 2. (b) Different values permeability, β_{\circ} , while setting $\nu = 0.3$ and R = 2, and (c) different separation distances, R, while setting $\nu = 0.3$ and $\beta_{\circ} = 5$. The time axis is made dimensionless with $\tau_D^R = R^2 \alpha_{\circ}^2 \tau_{\circ}$ in all the main plots. The inset figures in Fig. 4(c) show the same results as the main figure, but the time axes are made dimensionless with $\tau_D^A = a^2 \alpha_{\circ}^2 \tau_{\circ}$.

4.1. Slip boundary condition for the network phase

In deriving the expressions for the sphere's response to point-forces, we assumed no-slip BC for the network phase at the sphere's surface. This assumption generally holds when the size of the sphere is considerably larger than the network and there is no active interactions between the network and the sphere. As an example, the mesh-size for actin networks in the cell is roughly in the range $20 - 200 \, n$ m (Charras et al. 2005; Keren et al. 2009), and so the no-slip BC is appropriate for micron-sized endogenous bodies and injected probes used in microrheological measurements. But in many cases, such as transport of proteins and nanoscopic particles, the size of the inclusion can become comparable or smaller than the mesh size. In such conditions, we must account for slip velocity between the inclusion and the network phase (no-slip BC generally holds for the fluid phase down to atomistic lengths).

One method of modeling the slip velocity is to use the equivalent of Navier equation, where the tangential slip velocity is proportional to the traction in that direction:

$$v_n = \mathbf{U} + \frac{b}{\mu} (\mathbf{I} - \mathbf{n}\mathbf{n}) \cdot (\boldsymbol{\Sigma}_n \cdot \mathbf{n}),$$
 (4.1)

where b is the slip length, and μ is the term with dimensions of viscosity. Recall that the above equation is written in Laplace space. The time-dependence of μ depends on the mechanical coupling of the network with sphere's surface in microscopic scale. For example, if the network is not tethered to the boundary, we may assume that the slip dynamics is viscous, and take $\mu(t) = \mu_{\circ} \rightarrow \mu(s) = \mu_{\circ}/s$; in the opposite case of the network tethered to the boundary, the slip dynamics may be predominantly elastic,

leading to slip displacements rather than slip velocities: $\mu(t) = \mu_{\circ}\delta(t) \to \mu(s) = \mu_{\circ}$. In any case, we recover no-slip BC, when b = 0.

Our goal is to find the leading order correction to the force on a sphere moving with velocity \mathbf{U} , subject to this BC. We would like to avoid solving this boundary value problem by using the reciprocal theorem. We use the sphere moving with velocity $\hat{\mathbf{U}}$, with no-slip BC for both phases as our auxiliary problem, and use the slip BC for the network as our target solution. Upon substitution we find:

$$\mathbf{F} \cdot \hat{\mathbf{U}} = \hat{\mathbf{F}} \cdot \mathbf{U} + \left(\frac{b}{\mu}\right) \int_{S_n} \left(\hat{\boldsymbol{\Sigma}}_n \cdot \mathbf{n}\right) \cdot \left[(\mathbf{I} - \mathbf{n}\mathbf{n}) \cdot (\boldsymbol{\Sigma}_n \cdot \mathbf{n}) \right] dS.$$
(4.2)

Next, we assume small slip length $(\frac{b}{a} \ll 1)$, and so we can write down the following perturbation expansions:

$$\boldsymbol{v}_n = \hat{\boldsymbol{v}}_n + \left(\frac{b}{a}\right)\boldsymbol{v}_n^{(1)} + \mathcal{O}\left[\left(\frac{b}{a}\right)^2\right], \quad \boldsymbol{\Sigma}_n = \hat{\boldsymbol{\Sigma}}_n + \left(\frac{b}{a}\right)\boldsymbol{\Sigma}_n^{(1)} + \mathcal{O}\left[\left(\frac{b}{a}\right)^2\right]$$
 (4.3)

Substituting these expansions into Eq. (4.2), replaces Σ_n with $\hat{\Sigma}_n$, and so we get:

$$\mathbf{F} \cdot \hat{\mathbf{U}} = \hat{\mathbf{F}} \cdot \mathbf{U} + \left(\frac{b}{\mu}\right) \int_{S_p} \left[(\hat{\boldsymbol{\tau}}_n \cdot \hat{\boldsymbol{\tau}}_n) - (\hat{\boldsymbol{\tau}}_n \cdot \mathbf{n})^2 \right] dS + \mathcal{O} \left[\left(\frac{b}{a}\right)^2 \right], \tag{4.4}$$

where $\hat{\tau}_n = \hat{\Sigma}_n \cdot \mathbf{n}$ is the network traction of the auxiliary problem. We see that the reciprocal theorem can be used to compute the first order correction to the drag due to slip in the network phase. Almost the exact same derivation can be used to model slip BC in Stokes flow, as outlined in Masoud & Stone (2019).

When the inclusion is considerably smaller than the mesh $(b/a \gg 1)$, it can move through the network pores and channels without experiencing any force from the network. In this limit, no network traction, $\Sigma_n \cdot \mathbf{n} = 0$ at $|\mathbf{r}| = a$ would be a more appropriate BC. In this scenario and under a constant external force, the sphere will move with a steady-state velocity (viscous response) with the fluid velocity and the sphere's drag determined by Brinkman equation. In comparison, when no-slip BC is assumed for the network, as we showed earlier, the long-time behavior of the sphere under a constant force will be elastic.

Let's now consider the auxiliary problem of a sphere moving with velocity $\hat{\mathbf{U}}$, but this time with no-slip BC only applied to the fluid domain and zero traction BCs applied for the network phase. It is straightforward to find the displacement fields for this problem, using the general solutions of PVE equations (Moradi *et al.* 2022). Fu *et al.* (2008) also provide a closed form solution of this problem. Assuming that we have the solution for this auxiliary problem, we would like to find the net force on the sphere moving with velocity \mathbf{U} and subjected to point-forces in the fluid and network phases, using no traction from the network as BC. After substituting the auxiliary solution to the reciprocal theorem, and applying the BC, we recover Eqs. (3.6) and (3.7), with the distinction that $A_{\{f,n\}}$ and $B_{\{f,n\}}$ now correspond to the auxiliary problem with zero network traction as BC.

Finally, we ask if the combination of perturbation methods and the reciprocal theorem can be used to find the sphere's response functions to point-forces, subject to the slip BC given by Eq. (4.1). Again, we use the sphere moving with velocity $\hat{\mathbf{U}}$ with no-slip BCs for both phases as the auxiliary problem, and seek to find the net force on the sphere in response to point-forces $\mathbf{f}_{\{f,n\}} = \mathbf{f}_{\{f,n\}}^{\circ} \delta(\mathbf{r} - \mathbf{R})$, with the network BC given by Eq. (4.1).

After substitution and using $b/a \ll 1$ we get:

$$\mathbf{F} \cdot \hat{\mathbf{U}} = \hat{\mathbf{F}} \cdot \mathbf{U} + \hat{\mathbf{v}}_f(\mathbf{R}) \cdot \mathbf{f}_f^{\circ} + \hat{\mathbf{v}}_n(\mathbf{R}) \cdot \mathbf{f}_n^{\circ} + \left(\frac{b}{\mu}\right) \int_{S_p} \left(\hat{\boldsymbol{\Sigma}}_n \cdot \mathbf{n}\right) \cdot \left[(\mathbf{I} - \mathbf{n}\mathbf{n}) \cdot \left(\boldsymbol{\Sigma}_n^{(0)} \cdot \mathbf{n}\right) \right] dS + \mathcal{O}\left[\left(\frac{b}{a}\right)^2 \right]. \tag{4.5}$$

The first line of Eq. (4.5) is exactly the expression we get using no-slip BC in both phases. The second line shows the correction to the net force on the sphere due to network slip. Here, $\Sigma_n^{(0)}$ is the network stress in the target problem with no-slip BC in both phases. Thus, we see that using reciprocal theorem comes with the caveat of having to solve the problem of a sphere subjected to point-forces, with no-slip BC in both phases. Of course, the solution can be obtained, using the general solutions and the fundamental solutions to point-forces in the fluid and network phase. But the calculations are lengthy and will not be pursued here.

4.2. Nonlinearities in the fluid and network forces and stresses

Another utility of the reciprocal theorem in fluid mechanics is in calculating the leading order effects of nonlinear viscoelastic stresses (Leal 1980; Hu & Joseph 1999; Koch & Subramanian 2006; Khair & Squires 2010; Elfring 2015) and finite inertia (Ho & Leal 1974) in the net force and velocity of a particle, without the need to directly solve the nonlinear problem. See Masoud & Stone (2019) for a comprehensive review of the topic.

The same ideas can be directly applied to study the nonlinear effects in biphasic systems. To demonstrate this point, we reconsider the problem of a sphere moving a prescribed velocity **U** in an isotropic elastic network and a Newtonian fluid (with no-slip BC in both phases), and derive an expression that allows computing the leading order correction to the sphere's drag due to nonlinear terms that appear in the equations in finite deformations. One possible source of nonlinearity in the problem is the contribution of hyperelastic stresses in finite deformations of the elastic network. The simplest hyperelastic model is Saint Venant–Kirchhoff model (Nezamabadi et al. 2011), where a linear stress-strain relationship is still assumed and only geometric nonlinearities are accounted for. We choose this model for its simplicity, but the methodology can be directly used for other choices of hyperelastic models that reduce to linear elasticity in small deformations. In Saint Venant–Kirchhoff model the elastic stress in Eulerian coordinates is given by

$$\sigma_n = 2G e + \lambda \operatorname{trace}(e), \qquad e = \frac{1}{2} \left[\nabla u_n + (\nabla u_n)^T \right] - \nabla u_n \cdot (\nabla u_n)^T,$$
 (4.6)

where e is the Eulerian finite strain tensor, which also includes the nonlinear term that is the product of the displacement gradient and its transpose. Another source on nonlinearity is in the term that models the relative frictional forces between the fluid and network, $\xi(\partial u_n/\partial t - v_f)$. Specifically, the partial time derivative of the displacement field $(\partial u_n/\partial t)$ must be replaced with the velocity of material elements (Fu et al. 2010), which is defined as: $du_n/dt = \partial u_n/\partial t + (d/dt)(u_n(t) \cdot \nabla u_n(t))$.

We use perturbation expansion of the displacement and stress fields and the net force:

$$\boldsymbol{v}_{\{f,n\}} = \boldsymbol{v}_{\{f,n\}}^{(0)} + \boldsymbol{v}_{\{f,n\}}^{(1)}, \qquad \boldsymbol{\varSigma}_{\{f,n\}} = \boldsymbol{\varSigma}_{\{f,n\}}^{(0)} + \boldsymbol{\varSigma}_{\{f,n\}}^{(1)}, \qquad \mathbf{F} = \mathbf{F}^{(0)} + \mathbf{F}^{(1)},$$

and assume no-slip BC, which reduces to the following BCs for $v^{(0)}$ and $v^{(1)}$:

$$\boldsymbol{v}_{\{f,n\}}^{(0)}(|\mathbf{r}|=a)=\mathbf{U}, \qquad \qquad \boldsymbol{v}_{\{f,n\}}^{(1)}(|\mathbf{r}|=a)=\mathbf{0}.$$

The solution to the linear problem is known: $\mathbf{F}^{(0)} = -\mathcal{R}\mathbf{U}$. Importantly, $\mathbf{v}_{\{f,n\}}^{(1)}$ are also

described by linear biphasic equations with the difference that the equations also include body forces that are only dependent on the solution of the linear problem:

$$\nabla \cdot \boldsymbol{\Sigma}_{f}^{(1)} + \xi(\boldsymbol{v}_{n}^{(1)} - \boldsymbol{v}_{f}^{(1)}) = -\mathbf{f}_{f}, \quad \mathbf{f}_{f} = s\mathcal{L}\left[\boldsymbol{u}_{n}^{(0)}(t) \cdot \nabla \boldsymbol{u}_{n}^{(0)}(t)\right], \tag{4.7a}$$

$$\nabla \cdot \boldsymbol{\Sigma}_{n}^{(1)} - \xi(\boldsymbol{v}_{n}^{(1)} - \boldsymbol{v}_{f}^{(1)}) = -\mathbf{f}_{n}, \quad \mathbf{f}_{n} = \mathcal{L}\left[\nabla \cdot \boldsymbol{\sigma}_{n,\mathrm{n,l}}^{(0)}(t)\right] - s\mathcal{L}\left[\boldsymbol{u}_{n}^{(0)}(t) \cdot \nabla \boldsymbol{u}_{n}^{(0)}(t)\right], \tag{4.7b}$$

where $\boldsymbol{\sigma}_{n,\mathrm{n.l}}^{(0)} = -2G\left[\nabla \boldsymbol{u}_n^{(0)} \cdot (\nabla \boldsymbol{u}_n^{(0)})^T\right] - \lambda \operatorname{trace}\left[\nabla \boldsymbol{u}_n^{(0)} \cdot (\nabla \boldsymbol{u}_n^{(0)})^T\right]$ is the nonlinear piece of the elastic stress evaluated from the linear solution.

Next, we use the reciprocal theorem to find the drag contribution for the nonlinear terms, $\mathbf{F}^{(1)}$, without directly solving Eqs. (4.7). We use the solution to the linear problem with no body force as our auxiliary problem. Upon substitution we get

$$\mathbf{F} \cdot \hat{\mathbf{U}} = \int_{V} (\hat{\boldsymbol{v}}_f \cdot \mathbf{f}_f + \hat{\boldsymbol{v}}_n \cdot \mathbf{f}_n) \, dV, \tag{4.8}$$

where $\hat{\mathbf{U}} := \mathbf{U}$, $\mathbf{F} := \mathbf{F}^{(1)}$, and $\hat{\boldsymbol{v}}_{\{f,n\}} := \boldsymbol{v}_{\{f,n\}}^{(0)}$. Thus, $\mathbf{F}^{(1)}$ can be computed by evaluating the integral involving only known terms. Analytical evaluation of this integral is tedious, but the numerical integration is straightforward. The same methodology can be used to account for weak nonlinear stresses in the fluid phase, due to viscoelasticity (small Deborah numbers), or shear rate-dependent viscosity (Leal 1980; Elfring & Lauga 2015; Boyko & Stone 2021).

4.3. Self-propulsion in biphasic systems

Another major application of the reciprocal theorem is in modeling the self-propulsion of active biological or synthetic entities in low Reynolds number (Becker et al. 2003; Lauga & Powers 2009; Elfring 2015; Masoud & Stone 2014; Li et al. 2021). As with the previous examples, the framework in stokes flow can be directly extended to biphasic systems. We focus on the general case, where the active interactions between the motile object with the biphasic medium leads to slip velocities on the surface of the object with respect to the network and the fluid phases. The exact form of this slip velocity depends very much on the specifics of the involved active processes in smaller scales. For the purpose of this discussion we assume the slip velocities in both phases, $v_{\{f,n\}}^s$, are known. Our goal is to find the net propulsion speed of the force-free particle, \mathbf{U} , due to these surface activities. Hence, the velocity on the particle's surface is $v_{\{f,n\}} = \mathbf{U} + v_{\{f,n\}}^s$.

We use the solution to a particle moving with $\hat{\mathbf{U}}$ under no-slip BC as the auxiliary solution, and seek to find \mathbf{U} . After substitution we get:

$$\hat{\mathbf{F}} \cdot \mathbf{U} = -\int_{S_n} \left(\mathbf{v}_f^s \cdot \hat{\mathbf{\Sigma}}_f + \mathbf{v}_n^s \cdot \hat{\mathbf{\Sigma}}_n \right) \cdot \mathbf{n} \, \mathrm{d}S, \tag{4.9}$$

where we have used the force-free condition on the motile particle $(\int_{S_p} (\boldsymbol{\Sigma}_f + \boldsymbol{\Sigma}_n) \cdot \mathbf{n} \, dS = \mathbf{0})$ to derive the final expression. This expression holds for any particle shape. But, the expression is only useful, if the solution to the auxiliary problem is either known or can be obtained more easily using analytical and numerical methods. This formulation is also extendable to a collection of particles (Elfring 2015; Papavassiliou & Alexander 2015).

5. Summary

A reciprocal theorem was developed for a two-phase poro-viscoelastic (PVE) material composed of a linear compressible viscoelastic network that is permeated by a linear viscoelastic fluid. The theorem is expressed in Eq. (2.9) and, like its counterparts in stokes flow and linear elasticity, is applicable to anisotropic linear materials.

As an application of the reciprocal theorem, we analytically calculated the net force on a rigid stationary sphere due to point-forces in the fluid and network phases outside of the sphere. We chose the solution to a sphere moving with a prescribed velocity in the PVE medium (Moradi et al. 2022) as the auxiliary solution. We showed that the time evolution of the net force due to a point-force in a Newtonian fluid permeating a linear compressible elastic network is independent of the distance between the point-force and the sphere, and primarily determined by the diffusion time of network compressibility over lengths that scale with sphere radius: τ_D^a . In comparison, we found that the relaxation timescale of the net force on the sphere when the point-force is applied to the network is dependent on the distance of the point-force from the sphere, and at long times it is primarily determined by the diffusion time of network compressibility over lengths that scale with this distance: τ_D^R .

The reciprocal theorem can be applied to a variety of other problems. For example, the analysis involving calculating the net force on the sphere due to external point-forces in both phases can be readily extended to compute (a) the net stress (including pressure) on the sphere due to the same forces, (b) the net force on the sphere due to force dipoles on both phases, and (c) the stress on the sphere due to linear isotropic and shear displacement gradients in both phases. When combined with method of reflection (Happel & Brenner 2012), these results can be used to develop the mobility tensors for spherical inclusions in the same manner done in Stokes flow microhydrodynamics (Happel & Brenner 2012; Kim & Karrila 2013). These formulas can, then, be used to develop pseudo-analytical methods, such as Stokesian Dynamics (Fiore & Swan 2019) and its extensions (Swan et al. 2011) for computing the dynamics of a large assembly of particles. Furthermore, with some extra work these results can be extended from rigid spheres to viscous or poroelastic inclusions with more complex boundary conditions. These extensions can be useful for studying cell migration in tissues and the extracellular matrix or the dynamics of microswimmers in poroelastic media.

Another immediate application of our reciprocal theorem is to develop a boundary integral formulation of equations of motion in the same manner as Stokes flow (Pozrikidis 1992, 2002). Boundary integral methods can be used for fast and accurate simulations of the displacement and flow fields in the network and fluid phase containing many inclusions with complex geometry and dynamics. These numerical methods can be used in a wide range of problems in cell mechanics.

Appendix A. General solutions for axisymmetric spherical geometry

For the special case of the axisymmetric spherical geometry, the general solutions for the fluid and network velocity fields are (Moradi *et al.* 2022) $(A_{\ell}^{\pm}, B_{\ell}^{\pm}, C_{\ell}^{\pm}, C_{\ell}^{\prime\pm}, D_{\ell}^{\pm})$

(A 1a)

(A 2c)

and E_{ℓ}^{\pm} are constant coefficients):

$$v_{r,f} = \frac{1}{\eta + G} \left[\sum_{\ell=0}^{\infty} \left\{ A_{\ell}^{\pm} \begin{pmatrix} \ell r^{\ell-1} \\ -(\ell+1)r^{-\ell-2} \end{pmatrix} + B_{\ell}^{\pm} \frac{\ell(\ell+1)G}{\beta r} \begin{pmatrix} i_{\ell}(\beta r) \\ k_{\ell}(\beta r) \end{pmatrix} \right] \right]$$

$$+ D_{\ell}^{\pm} \begin{pmatrix} r^{\ell-1} \\ r^{-\ell-2} \end{pmatrix} \left(\frac{\ell}{2(2\ell+3)} r^2 - \frac{G}{\eta \beta^2} \ell \\ \frac{\ell+1}{2(2\ell-1)} r^2 + \frac{G}{\eta \beta^2} (\ell+1) \end{pmatrix} \right) P_{\ell}(\cos \theta)$$

$$v_{\theta,f} = \frac{1}{\eta + G} \left[\sum_{\ell=0}^{\infty} \left\{ A_{\ell}^{\pm} \begin{pmatrix} r^{\ell-1} \\ r^{-\ell-2} \end{pmatrix} + B_{\ell}^{\pm} \frac{G}{\beta} \left[\frac{d}{dr} \begin{pmatrix} i_{\ell}(\beta r) \\ k_{\ell}(\beta r) \end{pmatrix} + \frac{1}{r} \begin{pmatrix} i_{\ell}(\beta r) \\ k_{\ell}(\beta r) \end{pmatrix} \right] \right]$$

$$+ D_{\ell}^{\pm} \begin{pmatrix} r^{\ell-1} \\ r^{-\ell-2} \end{pmatrix} \left(\frac{\ell+3}{2(\ell+1)(2\ell+3)} r^2 - \frac{G}{\eta \beta^2} \right) \right\} \frac{d}{d\theta} P_{\ell}(\cos \theta)$$

$$+ D_{\ell}^{\pm} \begin{pmatrix} r^{\ell-1} \\ r^{-\ell-2} \end{pmatrix} \left(\frac{\ell+3}{2(\ell-1)} r^2 - \frac{G}{\eta \beta^2} \right) \right\} \frac{d}{d\theta} P_{\ell}(\cos \theta)$$

$$v_{r,n} = \frac{1}{\eta + G} \left[\sum_{\ell=0}^{\infty} \left\{ A_{\ell}^{\pm} \begin{pmatrix} \ell r^{\ell-1} \\ -(\ell+1)r^{-\ell-2} \end{pmatrix} - B_{\ell}^{\pm} \frac{\ell(\ell+1)\eta}{\beta r} \begin{pmatrix} i_{\ell}(\beta r) \\ k_{\ell}(\beta r) \end{pmatrix} \right] \right]$$

$$+ D_{\ell}^{\pm} \begin{pmatrix} r^{\ell-1} \\ r^{-\ell-2} \end{pmatrix} \left(\frac{\ell}{2(2\ell-3)} r^2 + \frac{1}{\beta^2} \ell \right)$$

$$+ D_{\ell}^{\pm} \begin{pmatrix} r^{\ell-1} \\ r^{-\ell-2} \end{pmatrix} \left(\frac{\ell}{2(2\ell-3)} r^2 + \frac{1}{\beta^2} \ell \right)$$

$$+ D_{\ell}^{\pm} \begin{pmatrix} r^{\ell-1} \\ r^{-\ell-2} \end{pmatrix} - B_{\ell}^{\pm} \frac{\eta}{\beta} \left[\frac{d}{dr} \begin{pmatrix} i_{\ell}(\beta r) \\ k_{\ell}(\beta r) \end{pmatrix} + \frac{1}{r} \begin{pmatrix} i_{\ell}(\beta r) \\ k_{\ell}(\beta r) \end{pmatrix} \right]$$

$$+ D_{\ell}^{\pm} \begin{pmatrix} r^{\ell-1} \\ r^{-\ell-2} \end{pmatrix} - B_{\ell}^{\pm} \frac{\eta}{\beta} \left[\frac{d}{dr} \begin{pmatrix} i_{\ell}(\beta r) \\ k_{\ell}(\beta r) \end{pmatrix} + \frac{1}{r} \begin{pmatrix} i_{\ell}(\alpha r) \\ k_{\ell}(\beta r) \end{pmatrix} \right]$$

$$+ D_{\ell}^{\pm} \begin{pmatrix} r^{\ell-1} \\ r^{-\ell-2} \end{pmatrix} - B_{\ell}^{\pm} \frac{\eta}{\beta} \left[\frac{d}{dr} \begin{pmatrix} i_{\ell}(\beta r) \\ k_{\ell}(\beta r) \end{pmatrix} + \frac{1}{r} \begin{pmatrix} i_{\ell}(\alpha r) \\ k_{\ell}(\beta r) \end{pmatrix} \right]$$

$$+ D_{\ell}^{\pm} \begin{pmatrix} r^{\ell-1} \\ r^{-\ell-2} \end{pmatrix} \left(\frac{\ell+3}{2(\ell+1)(2\ell+3)} r^2 + \frac{1}{\beta^2} \right) - \frac{\eta + G}{\alpha^2} E_{\ell}^{\pm} \frac{1}{r} \begin{pmatrix} i_{\ell}(\alpha r) \\ k_{\ell}(\alpha r) \end{pmatrix} \right\} \frac{d}{d\theta} P_{\ell}(\cos \theta)$$

$$+ D_{\ell}^{\pm} \begin{pmatrix} r^{\ell-1} \\ r^{-\ell-2} \end{pmatrix} \left(\frac{\ell+3}{2(\ell+1)(2\ell+3)} r^2 + \frac{1}{\beta^2} \right) - \frac{\eta + G}{\alpha^2} E_{\ell}^{\pm} \frac{1}{r} \begin{pmatrix} i_{\ell}(\alpha r) \\ k_{\ell}(\alpha r) \end{pmatrix} \right\} \frac{d}{d\theta} P_{\ell}(\cos \theta)$$

$$+ D_{\ell}^{\pm} \begin{pmatrix} r^{\ell-1} \\ r^{-\ell-2} \end{pmatrix} \left(\frac{\ell+3}{2(\ell+1)(2\ell+3)} r^2 + \frac{1}{\beta^2} \right) - \frac{\eta + G}{\alpha^2} E_{\ell}^{\pm} \frac{1}{r} \begin{pmatrix} i_{\ell}(\alpha r) \\ k_{\ell}(\alpha r) \end{pmatrix} \right\} \frac{d}{d\theta} P_{\ell}(\cos \theta)$$

$$+ D_{\ell}^{\pm} \begin{pmatrix} r^{\ell-1} \\ r^{-\ell-2} \end{pmatrix} \left(\frac{\ell+3}{2(\ell+1)(2\ell+3)} r^2 + \frac{1}{\beta^2} \end{pmatrix} - \frac{\eta + G}{\alpha^2} E_{\ell}^{\pm} \frac{1}{r} \begin{pmatrix} i_{\ell}(\alpha r) \\ k_{\ell}(\alpha r) \end{pmatrix} \right\} \frac{d}{d\theta} P_{\ell}(\cos \theta)$$

$$+$$

Here, $P_{\ell}(x)$ are the Legendre polynomials, and $i_{\ell}(x)$, and $k_{\ell}(x)$ are the modified spherical Bessel functions of first and second kind, respectively (Arfken & Weber 1999). For brevity, we have presented these solutions in the array format $()^{\pm}$. The first row contains the internal solutions (the functions are finite when $r \to 0$ and are unbounded as $r \to \infty$), and the second row contains the external solutions (the functions decay to zero as $r \to \infty$ and are singular as $r \to 0$). Also, the pressure is:

$$p = \sum_{\ell=0}^{\infty} \left\{ D_{\ell}^{\pm} \begin{pmatrix} r^{\ell} \\ r^{-\ell-1} \end{pmatrix} - (\lambda + 2G) E_{\ell}^{\pm} \begin{pmatrix} i_{\ell}(\alpha r) \\ k_{\ell}(\alpha r) \end{pmatrix} \right\} P_{\ell}(\cos \theta). \tag{A 3}$$

Acknowledgements. We thank the members of Nazockdast and Klotsa Labs for fruitful discussions and suggestions.

Funding. We acknowledge support by the National Science Foundation under Grant No. CBET-1944156.

Declaration of interest. The authors report no conflict of interest.

Author ORCIDs.

- Moslem Moradi https://orcid.org/0000-0001-9247-9351
- Wenzheng Shi https://orcid.org/0000-0002-1097-8497
- © Ehssan Nazockdast https://orcid.org/0000-0002-3811-0067

REFERENCES

- Abate, Joseph & Whitt, Ward 1992 The fourier-series method for inverting transforms of probability distributions. *Queueing systems* **10** (1), 5–87.
- ARFKEN, GEORGE B & WEBER, HANS J 1999 $Mathematical\ methods\ for\ physicists.$ American Association of Physics Teachers.
- Auriault, Jean-Louis 2009 On the domain of validity of Brinkman's equation. Transport in porous media 79 (2), 215–223.
- BECKER, LEIF E, KOEHLER, STEPHAN A & STONE, HOWARD A 2003 On self-propulsion of micro-machines at low reynolds number: Purcell's three-link swimmer. *Journal of fluid mechanics* **490**, 15–35.
- BIOT, MAURICE A 1941 General theory of three-dimensional consolidation. *Journal of applied physics* 12 (2), 155–164.
- BIOT, MAURICE A 1955 Theory of elasticity and consolidation for a porous anisotropic solid. *Journal of applied physics* **26** (2), 182–185.
- BOYKO, EVGENIY & STONE, HOWARD A 2021 Reciprocal theorem for calculating the flow rate—pressure drop relation for complex fluids in narrow geometries. *Physical Review Fluids* **6** (8), L081301.
- Brady, John F & Bossis, Georges 1988 Stokesian dynamics. Annual review of fluid mechanics ${f 20},\,111-157.$
- Burla, Federica, Mulla, Yuval, Vos, Bart E, Aufderhorst-Roberts, Anders & Koenderink, Gijsje H 2019 From mechanical resilience to active material properties in biopolymer networks. *Nature Reviews Physics* 1 (4), 249–263.
- Camley, Brian A & Rappel, Wouter-Jan 2017 Physical models of collective cell motility: from cell to tissue. *Journal of physics D: Applied physics* **50** (11), 113002.
- Carrillo, Francisco J & Bourg, Ian C 2019 A Darcy-Brinkman-Biot approach to modeling the hydrology and mechanics of porous media containing macropores and deformable microporous regions. *Water Resources Research* **55** (10), 8096–8121.
- Carrillo, Francisco J, Bourg, Ian C & Soulaine, Cyprien 2020 Multiphase flow modeling in multiscale porous media: An open-source micro-continuum approach. Journal of $Computational\ Physics:\ X\ 8,\ 100073.$
- CHARRAS, GUILLAUME T, COUGHLIN, MARGARET, MITCHISON, TIMOTHY J & MAHADEVAN, L 2008 Life and times of a cellular bleb. *Biophysical journal* **94** (5), 1836–1853.
- CHARRAS, GUILLAUME T, YARROW, JUSTIN C, HORTON, MIKE A, MAHADEVAN, L & MITCHISON, TJ 2005 Non-equilibration of hydrostatic pressure in blebbing cells. *Nature* 435 (7040), 365–369.
- Cheng, Alexander H-D 2016 Poroelasticity, , vol. 27. Springer.
- Cheng, Alexander H-D & Predeleanu, Mircea 1987 Transient boundary element formulation for linear poroelasticity. *Applied mathematical modelling* **11** (4), 285–290.
- Cowin, Stephen C & Doty, Stephen B 2007 $\it Tissue\ mechanics.$ Springer.
- CREMER, THOMAS, CREMER, MARION, HÜBNER, BARBARA, SILAHTAROGLU, ASLI, HENDZEL, MICHAEL, LANCTÔT, CHRISTIAN, STRICKFADEN, HILMAR & CREMER, CHRISTOPH 2020 The interchromatin compartment participates in the structural and functional organization of the cell nucleus. *BioEssays* 42 (2), 1900132.
- Detournay, Emmanuel & Cheng, Alexander H-D 1993 Fundamentals of poroelasticity. In *Analysis and design methods*, pp. 113–171. Elsevier.
- Doi, Masao 2009 Gel dynamics. Journal of the Physical Society of Japan 78 (5), 052001.
- Dumais, Jacques & Forterre, Yoël 2012 "vegetable dynamicks": the role of water in plant movements. *Annual Review of Fluid Mechanics* 44, 453–478.
- ELFRING, GWYNN J 2015 A note on the reciprocal theorem for the swimming of simple bodies. *Physics of Fluids* **27** (2), 023101.
- Elfring, Gwynn J & Lauga, Eric 2015 Theory of locomotion through complex fluids.

- Complex Fluids in Biological Systems: Experiment, Theory, and Computation pp. 283–317.
- Elfring, Gwynn J, Leal, L Gary & Squires, Todd M 2016 Surface viscosity and marangoni stresses at surfactant laden interfaces. *Journal of Fluid Mechanics* **792**, 712–739.
- ESTEKI, MOHAMMAD HADI, MALANDRINO, ANDREA, ALEMRAJABI, ALI AKBAR, SHERIDAN, GRAHAM K, CHARRAS, GUILLAUME & MOEENDARBARY, EMAD 2021 Poroelastic osmoregulation of living cell volume. *Iscience* 24 (12).
- FIORE, Andrew M & Swan, James W 2019 Fast stokesian dynamics. *Journal of Fluid Mechanics* 878, 544–597.
- FORTERRE, YOËL 2022 Basic soft matter for plants .
- Fu, Henry C, Shenoy, Vivek B & Powers, Thomas R 2008 Role of slip between a probe particle and a gel in microrheology. *Physical Review E* **78** (6), 061503.
- Fu, Henry C, Shenoy, Vivek B & Powers, Thomas R 2010 Low-reynolds-number swimming in gels. *Europhysics Letters* **91** (2), 24002.
- HAPPEL, JOHN & BRENNER, HOWARD 2012 Low Reynolds number hydrodynamics: with special applications to particulate media, , vol. 1. Springer Science & Business Media.
- Ho, BP & Leal, LG0284 1974 Inertial migration of rigid spheres in two-dimensional unidirectional flows. *Journal of fluid mechanics* **65** (2), 365–400.
- Hobson, Chad M, Falvo, Michael R & Superfine, Richard 2021 A survey of physical methods for studying nuclear mechanics and mechanobiology. *APL bioengineering* **5** (4), 041508.
- HOWARD, JONATHON 2001 Mechanics of motor proteins and the cytoskeleton. Sinauer associates Sunderland, MA.
- Hu, Howard H & Joseph, Daniel D 1999 Lift on a sphere near a plane wall in a second-order fluid. *Journal of non-newtonian fluid mechanics* 88 (1-2), 173–184.
- Jiang, Hongyuan & Sun, Sean X 2013 Cellular pressure and volume regulation and implications for cell mechanics. *Biophysical journal* **105** (3), 609–619.
- Kalukula, Yohalie, Stephens, Andrew D, Lammerding, Jan & Gabriele, Sylvain 2022 Mechanics and functional consequences of nuclear deformations. *Nature reviews Molecular cell biology* **23** (9), 583–602.
- KEREN, KINNERET, YAM, PATRICIA T, KINKHABWALA, ANIKA, MOGILNER, ALEX & THERIOT, JULIE A 2009 Intracellular fluid flow in rapidly moving cells. *Nature cell biology* **11** (10), 1219–1224.
- Khair, Aditya S & Squires, Todd M 2010 Active microrheology: a proposed technique to measure normal stress coefficients of complex fluids. *Physical review letters* **105** (15), 156001
- Kim, Sangtae & Karrila, Seppo J 2013 Microhydrodynamics: principles and selected applications. Courier Corporation.
- KOCH, DONALD L & SUBRAMANIAN, G 2006 The stress in a dilute suspension of spheres suspended in a second-order fluid subject to a linear velocity field. *Journal of non-newtonian fluid mechanics* 138 (2-3), 87–97.
- Lauga, Eric & Powers, Thomas R 2009 The hydrodynamics of swimming microorganisms. Rep. Prog. Phys 72 (096601), 096601.
- Leal, LG 1980 Particle motions in a viscous fluid. Annual Review of Fluid Mechanics 12 (1), 435–476.
- LEVINE, ALEX J & LUBENSKY, TC 2000 One-and two-particle microrheology. Physical review letters $\bf 85$ (8), 1774.
- Levine, Alex J & Lubensky, TC 2001 Response function of a sphere in a viscoelastic two-fluid medium. *Physical Review E* **63** (4), 041510.
- LÉVY, Thérese 1983 Fluid flow through an array of fixed particles. *International Journal of Engineering Science* **21** (1), 11–23.
- LI, GAOJIN, LAUGA, ERIC & ARDEKANI, AREZOO M 2021 Microswimming in viscoelastic fluids. Journal of Non-Newtonian Fluid Mechanics 297, 104655.
- MARCHETTI, M CRISTINA, JOANNY, JEAN-FRANÇOIS, RAMASWAMY, SRIRAM, LIVERPOOL, TANNIEMOLA B, PROST, JACQUES, RAO, MADAN & SIMHA, R ADITI 2013 Hydrodynamics of soft active matter. *Reviews of modern physics* 85 (3), 1143.

- MASOUD, HASSAN & STONE, HOWARD A 2014 A reciprocal theorem for marangoni propulsion. Journal of Fluid Mechanics 741, R4.
- MASOUD, HASSAN & STONE, HOWARD A 2019 The reciprocal theorem in fluid dynamics and transport phenomena. *Journal of Fluid Mechanics* 879.
- MITCHISON, TJ, CHARRAS, GT & MAHADEVAN, L 2008 Implications of a poroelastic cytoplasm for the dynamics of animal cell shape. In *Seminars in cell & developmental biology*, , vol. 19, pp. 215–223. Elsevier.
- MOEENDARBARY, EMAD, VALON, LÉO, FRITZSCHE, MARCO, HARRIS, ANDREW R, MOULDING, DALE A, THRASHER, ADRIAN J, STRIDE, ELEANOR, MAHADEVAN, L & CHARRAS, GUILLAUME T 2013 The cytoplasm of living cells behaves as a poroelastic material. *Nature materials* 12 (3), 253.
- MOGRE, SAURABH S, BROWN, AIDAN I & KOSLOVER, ELENA F 2020 Getting around the cell: physical transport in the intracellular world. *Physical Biology* **17** (6), 061003.
- MORADI, MOSLEM, SHI, WENZHENG & NAZOCKDAST, EHSSAN 2022 General solutions of linear poro-viscoelastic materials in spherical coordinates. *Journal of Fluid Mechanics* **946**, A22.
- NEZAMABADI, SAEID, ZAHROUNI, HAMID & YVONNET, JULIEN 2011 Solving hyperelastic material problems by asymptotic numerical method. *Computational mechanics* 47 (1), 77–92.
- Papavassiliou, Dario & Alexander, Gareth P 2015 The many-body reciprocal theorem and swimmer hydrodynamics. *Europhysics Letters* **110** (4), 44001.
- Phan-Thien, Nhan & Kim, Sangtae 1994 Microstructures in elastic media: principles and computational methods. Oxford University Press, USA.
- Pozrikidis, Constantine 1992 Boundary integral and singularity methods for linearized viscous flow. Cambridge university press.
- Pozrikidis, Constantine 2002 A practical guide to boundary element methods with the software library BEMLIB. CRC Press.
- PREDELEANU, MIRCEA 1984 Development of boundary element method to dynamic problems for porous media. Applied mathematical modelling 8 (6), 378–382.
- Saintillan, David & Shelley, Michael J 2015 Theory of active suspensions. Complex Fluids in Biological Systems: Experiment, Theory, and Computation pp. 319–355.
- SHANKAR, SURAJ & MAHADEVAN, L 2022 Active muscular hydraulics. bioRxiv pp. 2022–02.
- SIMON, BRUCE R 1992 Multiphase poroelastic finite element models for soft tissue structures .
- Stone, Howard A & Samuel, Aravinthan DT 1996 Propulsion of microorganisms by surface distortions. *Physical review letters* **77** (19), 4102.
- Strychalski, Wanda, Copos, Calina A, Lewis, Owen L & Guy, Robert D 2015 A poroelastic immersed boundary method with applications to cell biology. *Journal of Computational Physics* 282, 77–97.
- SWAN, JAMES W, BRADY, JOHN F, MOORE, RACHEL S & OTHERS 2011 Modeling hydrodynamic self-propulsion with stokesian dynamics. or teaching stokesian dynamics to swim. *Physics of Fluids* 23 (7).
- Weihs, Daphne, Mason, Thomas G & Teitell, Michael A 2006 Bio-microrheology: a frontier in microrheology. *Biophysical journal* 91 (11), 4296–4305.